Bioconjugate Chemistry

Article

pubs.acs.org/bc

Bioresorbable Polymersomes for Targeted Delivery of Cisplatin

Matthew A. Petersen,[†] Marc A. Hillmyer,[‡] and Efrosini Kokkoli*[,†]

[†]Department of Chemical Engineering and Materials Science, [‡]Department of Chemistry, University of Minnesota, Minneapolis, Minnesota 55455, United States

Supporting Information

ABSTRACT: Nontoxic bioresorbable polymersomes have been developed that efficiently and site-selectively tether targeting peptides under mild conditions with no toxic catalysts. The binding and release properties of these polymersomes have been evaluated when targeting DLD-1 human colon cancer cells overexpressing the $\alpha_5\beta_1$ integrin. The delivery efficacy to these cells is markedly improved over commonly used RGD targeting peptides by use of an $\alpha_5\beta_1$-specific targeting peptide, PR_b. Release profiles in buffered solution from pH 7.4 to 4.5 were evaluated and compared to release after binding to cells, and enzymatic degradation was identified as a major cause of rapid payload release in the cell. Intracellular trafficking and release were imaged *via* confocal microscopy in live cells and colocalization with organelles was evaluated quantitatively over time. Finally, the anticancer drug cisplatin was encapsulated in the PR_b functionalized polymersomes and the presence of PR_b greatly improved delivery efficacy, with increased cisplatin-induced losses to targeted DLD-1 colon cancer cell viability. When delivered to CACO-2 model human epithelial cells expressing low levels of $\alpha_5\beta_1$ integrin, low toxicity was maintained, suggesting that targeting was specific to $\alpha_5\beta_1$ overexpressing cells. These results demonstrate that PR_b-functionalized bioresorbable polymersomes may be an attractive route to minimizing the dose-limiting side effects associated with existing approaches to cisplatin chemotherapy.

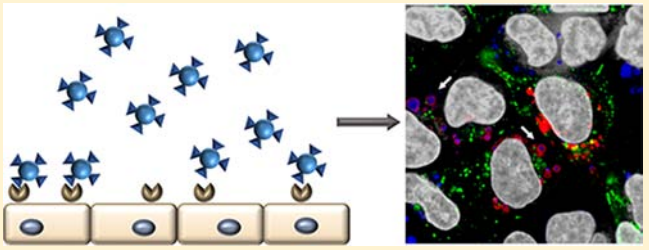

INTRODUCTION

Chemotherapy today is often limited by deleterious side effects from drug toxicity to healthy tissue encountered en route to cancer cells. A wide range of carriers have been developed to deliver more active agents to cancer cells while minimizing drug concentrations elsewhere in the body.[1−4] Like many carriers, polymersomes' densely packed surface of hydrophilic polymer and facile size adjustment via techniques such as extrusion to 100−200 nm allow long circulation *in vivo* and enhanced intratumoral accumulation via the enhanced permeability and retention (EPR) effect.[5−7] Uniquely, polymersomes' combination of thick hydrophobic shell and aqueous lumen allows simultaneous encapsulation of large quantities of both hydrophilic and hydrophobic drugs, positioning them among the most versatile drug delivery vehicles.[8−11]

Early polymersomes were assembled from nondegradable polymers with no clear mechanism for releasing cargo or clearance from the body following delivery.[8,9,12] More recently, several groups have developed polymersomes with biodegradable or stimulus-responsive properties.[13−19] We have focused our attention on the block polymer poly(ethylene oxide)-*b*-poly(γ-methyl-ε-caprolactone) (PEO-PMCL)—a low T_g amorphous polyester that forms polymersomes with simple stirring in water at room temperature—and its reactive vinyl sulfone-functionalized analog (VS-PEO-PMCL), which can site-specifically tether targeting peptides with high yield in mild conditions after self-assembly.[20−22] In many cases, the release profile and mechanism of release for both degradable and nondegradable polymersomes have not been compared between simple solution release experiments and the conditions encountered following cellular uptake, resulting in ambiguity regarding the performance of these carriers.

One of the most appealing drugs for encapsulation in a polymersome is the water-soluble drug cisplatin, as it is limited clinically by side effects including damage to the kidneys, nervous system, auditory system, bone marrow, and digestive system.[23,24] Further, cisplatin-resistant cancers are well-documented, markedly diminishing the effectiveness of treatment *via* decreased drug uptake, increased drug efflux, intracellular inactivation, or enhanced DNA repair, among others.[25,26] Many approaches to cisplatin using delivery vehicles have been investigated to diminish the side effects associated with nonspecific delivery.[27,28] One of the most promising, cisplatin encapsulated in "stealth" liposomes, increased the amount of the drug that could be administered without major side effects and significantly increased platinum concentration in the tumor.[29−32] Despite these promising inroads, therapy using the system proved to be ineffective due to the lack of a route for sufficient drug to reach the interior of target cells for effective therapy; though liposomes and encapsulated drug had accumulated in the vicinity of cancer cells there was no way for

Received: June 19, 2012
Revised: February 25, 2013
Published: March 22, 2013

   dx.doi.org/10.1021/bc3003259 | *Bioconjugate Chem.* 2013, 24, 533−543

drug to be delivered to the interior of cells, a crucial final step for administered drug to be effective.[33−37]

To surmount this barrier, active targeting techniques have been explored to deliver cisplatin to the cell interior using a variety of targeting ligands to bind cancer cells and deliver drug. These also have the advantage of potentially circumventing some modes of drug resistance by leveraging alternate routes to internalization.[25,26,38−45] Perhaps the most commonly used ligand for targeted drug delivery is the RGD peptide sequence, which is derived from the extracellular matrix protein fibronectin and capable of binding several integrins overexpressed on certain cancer cells.[46−48]

While the RGD sequence has proven quite effective in enhancing delivery, it has the potential to bind a variety of integrins, hindering delivery specificity. To address this concern, we instead have aimed to target the $\alpha_5\beta_1$ integrin specifically. Highly expressed in embryos but only minimally expressed in healthy adult vasculature,[49] specific targeting of the $\alpha_5\beta_1$ integrin is promising due to the integrin's overexpression in cancers of the breast, prostate, colon, skin, lung, and rectum and low levels of expression elsewhere.[50−58] As a result, specific targeting to this integrin using a high-affinity ligand has the potential to enhance treatment outcomes by binding specifically to diseased cells. To achieve this goal, the PR_b peptide was developed by mimicking the cell adhesion domain of fibronectin, the native ligand of integrin $\alpha_5\beta_1$. This peptide was designed to include fibronectin's RGD binding and PHSRN synergy sites while separating the two by an $(SG)_5$ linker mimicking the hydrophobicity/hydrophilicity and separation between these two domains on native fibronectin.[59−62] Blocking experiments with antibodies have demonstrated that PR_b is a specific ligand for the $\alpha_5\beta_1$ integrin[62,63] and with a dissociation constant of 76.3 ± 6.3 nM[64] PR_b enhances binding and payload delivery when tethered to a delivery vehicle.[12,65−71] The development of such a specific and high-affinity ligand suggests a role for a versatile carrier capable of enhanced tumor accumulation via the EPR effect, specific internalization to the interior of cancer cells via binding between PR_b and the $\alpha_5\beta_1$ integrin, and a clear means of release from nanoparticles such as the PEO-PMCL polymersomes described here.

Herein the characterization and use of targeting PEO-PMCL polymersomes is reported as a delivery system for cisplatin. The role of the targeting ligand was investigated, demonstrating that compared to simple RGD peptides, the PR_b peptide promoted enhanced binding to $\alpha_5\beta_1$-overexpressing cancer cells, such as DLD-1, with no binding to CACO-2 cells (CACO-2 is an intestinal epithelial cell line that is known to express low levels of $\alpha_5\beta_1$ integrin).[63,72−77] Release of a model drug from these peptide-functionalized polymersomes was then tracked and release profiles were compared between simple buffered solutions and after binding and internalization into cells, exploring the effects of hydrolases on intracellular release. Intracellular trafficking and release of polymersomes in live cells were then observed *via* confocal microscopy to quantitatively study payload colocalization with intracellular organelles.[78] Finally, treatment efficacy was compared between free cisplatin and polymersomes encapsulating the drug to determine the effect of targeting using a conventional RGD-based targeting peptide and the PR_b ligand. Results indicate that targeted delivery using PR_b dramatically enhanced specific delivery of cisplatin to $\alpha_5\beta_1$-overexpressing DLD-1 human colon cancer cells but not to CACO-2 cells relative to nontargeted formulations.

EXPERIMENTAL SECTION

Materials. All chemicals were obtained from Sigma-Aldrich (St. Louis, MO) and used as received unless otherwise noted. Polymers were synthesized according to previously described procedures and were composed of a poly(ethylene oxide) (PEO) block with a number average molecular weight of 2 kg mol^{-1} and a poly(γ-methyl-ε-caprolactone) (PMCL) block with a number average molecular weight of 9 kg mol^{-1} for both the nonreactive polymer (PEO-PMCL) and the vinyl-sulfone modified reactive polymer (VS-PEO-PMCL).[20,21,79] Water was obtained from a Milli-Q water system purified to a resistivity of 18.2 MΩ cm. Unless otherwise specified, all phosphate buffered saline (PBS) was 100 mM and pH 7.4. Phosphate-citrate buffers were prepared using appropriate combinations of dibasic sodium phosphate and citric acid for the desired pH and ionic strength adjusted to match the polymersome interior using sodium chloride. Peptides cPR_b (CKSSPHSRNSGSGSGSGSGRGDSP) and cGRGDSP (CGRGDSP) were synthesized by the Oligonucleotide and Peptide Synthesis Facility at the University of Minnesota. Antibodies were purchased from Millipore (Billerica, MA). Fluorescence readings were acquired using a Beckman Coulter DTX 880 spectrophotometer. Hoechst 33342 nucleic acid stain, CellLights Early Endosome-GFP (Rab5-GFP), and CellLights Lysosome-RFP (LAMP1-RFP) were obtained from Invitrogen (Carlsbad, CA). Fetal bovine serum (FBS) was purchased from Atlas Biologicals (Fort Collins, CO).

Polymersome Preparation and Characterization. Polymersomes were prepared at 1 wt/vol% polymer in water using thin-film hydration followed by peptide conjugation as described previously.[20] All targeting polymersomes were formulated to incorporate 10 mol % VS-PEO-PMCL polymer and 90% PEO-PMCL, resulting in a final peptide concentration of 9 mol % on the vesicle exterior. The disparity between incorporated reactive polymer and final peptide concentration was attributed primarily to vinyl sulfone hydrolysis during polymer purification and vesicle formation. Cisplatin, sulforhodamine B, and calcein blue were encapsulated by dissolution at the desired concentration in the suspension media during polymersome formation. After at least 7 days of stirring, samples were subjected to 10 freeze−thaw cycles using liquid nitrogen and a water bath at ∼65 °C and unincorporated drug and peptide removed *via* filtration through a Sepharose CL-4B column using an Amersham Acta Fast Protein Liquid Chromatograph at 0.85 mL s^{-1}. To ensure that the same amount of encapsulated payload was delivered in experiments testing binding, release, and toxicity, encapsulated dye was quantified by lysing a known volume of purified polymersomes and measuring fluorescence. Platinum concentrations were determined using *o*-phenylenediamine.[80] Encapsulation efficiency for cisplatin ranged from 3% to 5%, which is on the lower side of the efficiencies reported for other polymersomal systems.[10,81,82] The size of the nanoparticles was characterized by Nanoparticle Tracking Analysis (NTA) using a NanoSight LM10-HSBT14 Nanoparticle Characterization System with a 640 nm laser and a high resolution CCD camera. Each of the three polymersome formulations used for the measurements was diluted approximately 1000-fold into pH 7.4 phosphate buffered saline and injected into the sample flow cell maintained at 23.3 °C using clean syringes. Measurements

were performed for 60 s five times for each sample using a detection threshold of 5 and automatic shutter and gain adjustment. Size and standard deviation were determined from these pooled results assuming spherical particles.

Cell Culture. DLD-1 human colon cancer cells were grown in growth media (GM: RPMI 1640 supplemented with 10% FBS and 1% penicillin/streptomycin) in an incubator maintained at 37 °C and 5% CO_2. Cells were kept in T-75 flasks and fed every 2 days. When cells reached approximately 90% confluence they were washed twice with PBS, trypsinized (1 mL 0.25% trypsin with 0.1% ethylenediaminetetraacetic acid), resuspended in GM, and seeded at 10^6 cells per flask. For CACO-2 cells the same procedure was used with GM containing 20% FBS.

Flow Cytometry. DLD-1 cells were grown to 90% confluence, trypsinized, and 10^6 cells suspended in three microcentrifuge tubes each containing 1 mL fluorescence buffer (FB: PBS with 0.02% sodium azide and 2.5% FBS) at 0 °C. Mouse IgG was added to one tube for isotype control and mouse antihuman integrin $\alpha_5\beta_1$was added to a second tube. All three tubes were placed on a rotary shaker for 35 min at 4 °C. All three were pelleted, washed twice with FB, and resuspended in 1 mL FB. Secondary antibody (5 μL donkey antimouse IgG-FITC) was added to the isotype control and $\alpha_5\beta_1$ tubes and mixed by rotary shaker at 4 °C for an additional 40 min. All tubes were again washed twice in FB and resuspended in 1 mL FB. Flow cytometry was performed using a FACSCalibur flow cytometer at the Flow Cytometry Core facility in the Cancer Research Center at the University of Minnesota. 1.5×10^4 cells were counted for each curve.

Viability Assays. Cells were seeded onto polystyrene plates at 2×10^5 cells per well and allowed to attach overnight in GM. The media was then removed, fresh GM added, and polymersomes containing either PBS or cisplatin were added at the desired concentrations. Plates were returned to the incubator for 24 h. Following this incubation, GM and polymersomes were removed, plates were washed twice with warm PBS, fresh GM was added, and plates were returned to the incubator for 2 days. After 2 days the MTT assay was performed according to the recommendations of the manufacturer (Sigma-Aldrich), with measurements of optical density taken using a Molecular Devices Spectramax Plus 384 spectrophotometer. Viability curves were fit to a sigmoidal curve to determine 50% inhibition concentrations (IC_{50}) using untreated cells to establish 0% inhibition. Representative curves can be found in the Supporting Information, Figure S5.

Binding Assay. Cells were plated at 10^6 cells per well in a white-bottomed 96-well plate and allowed to adhere for 18 h. The media was then exchanged for 100 μL of fresh GM. Free peptide was added at various concentrations and GM was added so all wells were 125 μL. 15 μL of polymersomes containing 2 mM sulforhodamine B was added and plates were returned to the incubator for 1 h. Polymersome solutions were diluted as necessary using isotonic PBS to ensure equal dye concentrations were delivered to all wells. Plates were washed 3 times with PBS to remove unbound polymersomes and 100 μL fresh GM was added to each well. Fluorescence measurements were taken at 37 °C using an excitation wavelength of 535 nm and an emission wavelength of 595 nm. Wells that contained approximately the same number of cells but to which no dye had been added were used to account for autofluorescence.

Solution Release Assay. To evaluate release as a function of pH, polymersomes containing 100 mM sulforhodamine B were formed and purified as described above. Phosphate-citrate buffer was formulated to pH 7.4, 6.5, 5.5 and 4.5. 150 μL of each buffer was added to separate wells of a 96 well plate and to these 1 μL of purified polymersome solution was added. Fluorescence was then measured over time. After 24 h, wells were frozen at −80 °C for 2 h, thawed at 37 °C for 2 h, and final fluorescence measured. Wells to which no polymersomes were added were used to account for background fluorescence.

Intracellular Release Assay. DLD-1 cells were plated at 10^6 per well in a 96-well plate and allowed to adhere for 18 h in GM. The media was then exchanged for 100 μL of fresh GM with or without 500 μM chloroquine. Polymersomes were immediately added, diluting as necessary to ensure equal dye concentrations were added, and after gentle shaking plates were returned to the incubator for 30 min. Wells were then washed twice with warm GM and 150 μL fresh GM was added to each well, with those wells previously containing chloroquine again supplemented with the drug to 500 μM. Fluorescence was measured immediately and again at 2 h, 8 h, and 24 h as described above. Plates were then placed in a −80 °C freezer for 2 h then thawed for 2 h at 37 °C. Final fluorescence was then measured. To control for autofluorescence, wells with polymersomes without fluorescent dye were included. Non-specific adhesion of polymersomes to the plate was not found to result in significant fluorescence. Chloroquine was verified to not affect cell viability in the concentration ranges used in this experiment (Supporting Information, Figure S4).

Confocal Microscopy. DLD-1 cells were seeded onto a glass-bottomed 24-well plate at 5×10^4 cells per well in 200 μL GM per well and allowed to attach overnight in an incubator. Media was then exchanged for 200 μL fresh GM in each well. Wells to be used for imaging received 2.5 μL of CellLights early endosomes-GFP and 7.5 μL CellLights lysosome-RFP, the media mixed, and the cells returned to the incubator for 18 h. Following incubation, 25 μL purified cPR_b-functionalized polymersomes containing either nonquenching (5 mM) or quenching (100 mM) concentrations of calcein blue were added. After 2 h incubation at 37 °C, media was removed and each well washed twice with warm GM. 2 h wells were immediately nuclear stained while 150 μL GM was added to 24 h wells. Immediately prior to imaging, media was replaced with 100 μL warm GM containing diluted Hoechst 33342 at 1 μM, which was allowed to stain nuclei for 5 min at 37 °C. These wells were washed twice with warm GM and finally filled with 150 μL GM prior to imaging.

Imaging was performed on a Zeiss Cell Observer SD spinning disk confocal microscope at 37 °C and 5% CO_2 at the University of Minnesota Biomedical Image Processing Lab. A 100× objective was used, using the green channel for GFP-tagged early endosomes, the red channel for RFP-tagged lysosomes, and the blue channel for both nuclei and calcein blue. Slices were taken every 0.25 μm from the bottom to the top of cells, collecting each channel in series for each slice. A slice at the center of the cell was used for analysis and the Manders coefficients between blue-green and blue-red determined accounting for background fluorescence, according to the Costes technique in NIH ImageJ and gating out nuclei so as to consider only polymersomes.[83,84] Sample movies of cells interacting with polymersomes can be found in the Supporting Information, Movies S1 and S2.

RESULTS AND DISCUSSION

Particle size and prolonged circulation are vital for enhancing the carrier concentration in tumors; however, the EPR effect is only effective for localizing the delivery vehicle to the tumor interstitium, not for achieving internalization. This last step has proven to be a major stumbling block for past attempts to deliver cisplatin.[33−37] To achieve internalization, active targeting groups show great promise, using ligands tethered to the delivery vehicle to take advantage of the cell's existing uptake pathways and overexpression of cell-surface receptors, affording a route for selective internalization and potentially circumventing some modes of cisplatin resistance and allowing selective binding and uptake of several nanoparticle-based cisplatin carriers.[25,26,38−44,85]

Active targeting was incorporated into PEO-PMCL polymersomes using a vinyl sulfone moiety capable of site-specifically tethering a targeting peptide following self-assembly (Figure 1).

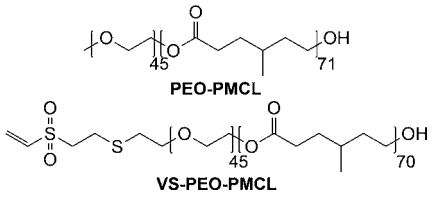

Figure 1. Schematic of the block copolymers PEO-PMCL and VS-PEO-PMCL that self-assemble in water into polymersomes capable of encapsulating both hydrophilic and hydrophobic payloads. The vinyl sulfone moiety allows selective conjugation, after self-assembly, to thiol-containing targeting ligands. Numbers outside of brackets indicate the number-average degree of polymerization as determined by ^{1}H NMR.

Due to compatibility between PEO-PMCL and VS-PEO-PMCL and the high reactivity between vinyl sulfone and thiol-containing peptides, the amount of targeting peptide incorporated into the corona can be easily controlled, here using either 0 or 9 mol % peptide by mixing appropriate ratios of the two polymers prior to self-assembly. The critical aggregation concentration (CAC) for PEO-PMCL was found to be 0.38 ± 0.06 μM (Supporting Information, Figure S2). The size of the nanoparticles was characterized by Nanoparticle Tracking Analysis, NTA, (representative histograms are shown in Supporting Information, Figure S3). Results are shown in Table 1 and are in agreement with cryo-TEM images taken previously.[20]

Table 1. Hydrodynamic Diameter of the Polymersomes as Determined Using NTA (n = 3)

sample	size ± SD (D_h, nm)
Nontargeted	217 ± 63
cGRGDSP	214 ± 62
cPR_b	234 ± 45

The chemical similarity of PEO-PMCL to the more commonly studied and biocompatible PEO-poly(ε-caprolactone)[86,87] suggests PEO-PMCL would also be nontoxic. The effect of both nontargeted and targeted PEO-PMCL polymersomes on the viability of DLD-1 human colon cancer cells was determined. As shown in Figure 2, neither targeted nor nontargeted PEO-PMCL polymersomes impacted cell viability following a 24 h incubation period with unloaded polymersomes. High viability was observed even at concentrations much greater than the 0.8 mg/mL maximum concentration of polymersomes used in this work, indicating that the polymer should have no impact on cellular viability.

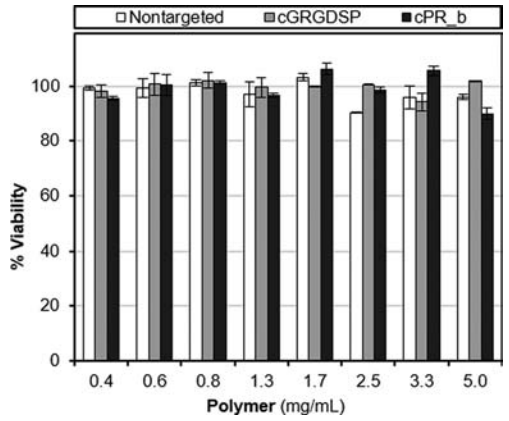

Figure 2. Toxicity of empty polymersomes to the DLD-1 human colon cancer cells was evaluated with an MTT viability assay after 24 h of incubation at 37 °C. While in the rest of this work polymer concentrations never exceeded 0.8 mg/mL, no significant decrease in viability was observed even at much higher concentrations. Data is the mean ± standard error of 4 separate experiments (n = 4), with each experiment performed in triplicate.

To evaluate binding specificity DLD-1 and CACO-2 human colon cancer cells with different levels of $\alpha_5\beta_1$ expression were used and evaluated via flow cytometry with an antihuman $\alpha_5\beta_1$ antibody (Figure 3). While some expression was observed in CACO-2 (Figure 3B), the pronounced shift toward higher fluorescence in DLD-1 (Figure 3A) indicated that $\alpha_5\beta_1$ expression was much greater in the latter cell line.

To minimize the negative side effects of chemotherapy it is essential that binding of the delivery vehicle occurs with high specificity for the target cells. To determine if employing a high-affinity targeting peptide such as cPR_b would yield improved binding to $\alpha_5\beta_1$-overexpressing cancer cells, the effect of the targeting ligand on the binding of polymersomes to DLD-1 cells was evaluated (Figure 4A). Here, minimal binding occurred in the absence of a targeting peptide, a pronounced increase when the cGRGDSP peptide was used, and a maximum effect using the cPR_b peptide. Further, this binding could be inhibited by including free cGRGDSP peptide in media, which hindered the interaction between the peptides and integrins. Across all experiments using nontargeted polymersomes the peptide concentration of the free cGRGDSP in the media was not found to have a statistically significant effect on fluorescence. To determine if the binding to cells with lower expression of $\alpha_5\beta_1$ integrin would be significant, the same experiment was performed using low-$\alpha_5\beta_1$-expressing CACO-2 cells, a cell line often used as a model of intestinal epithelia.[63,72−77] Little or no binding enhancement was observed using targeted polymersomes compared to nontargeted regardless of the concentration of the blocking peptide. These results suggest that polymersomes functionalized with the cPR_b sequence can promote delivery to the cancer cells of interest that overexpress the $\alpha_5\beta_1$ integrin with minimal delivery to bystander cells even if they express low levels of the integrin.

To evaluate the release properties of PEO-PMCL polymersomes, studies were first conducted in simple buffered solution at pH values from 7.4 to 4.5 (Figure 5A), levels commonly used to simulate the decreasing pH level encountered by a drug

dx.doi.org/10.1021/bc3003259 | Bioconjugate Chem. 2013, 24, 533−543

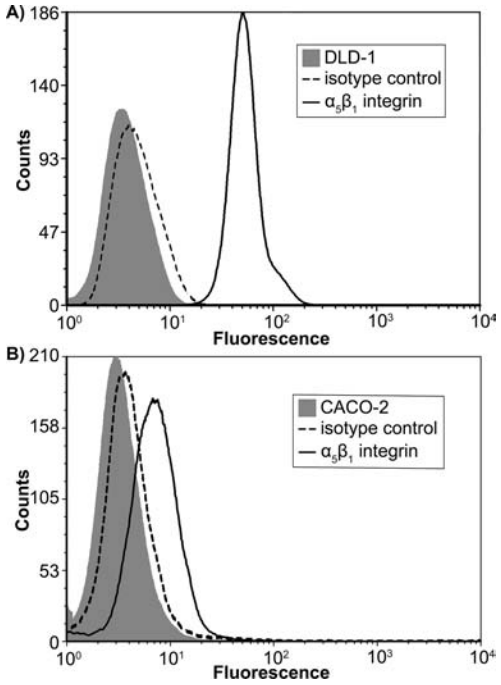

Figure 3. Histograms of flow cytometry used to determine expression of $\alpha_5\beta_1$ integrin, the target of cPR_b peptide, on (A) DLD-1 and (B) CACO-2 cell lines. Untreated cells were used to measure cell autofluorescence and an isotype control was included to verify that binding was specific. The pronounced shift to higher fluorescence values in DLD-1 cells—but not in CACO-2—following incubation with an antibody specific to $\alpha_5\beta_1$ integrin is indicative of much higher expression of the integrin on DLD-1 cells. These data are from a single experiment but are representative of $n = 2$.

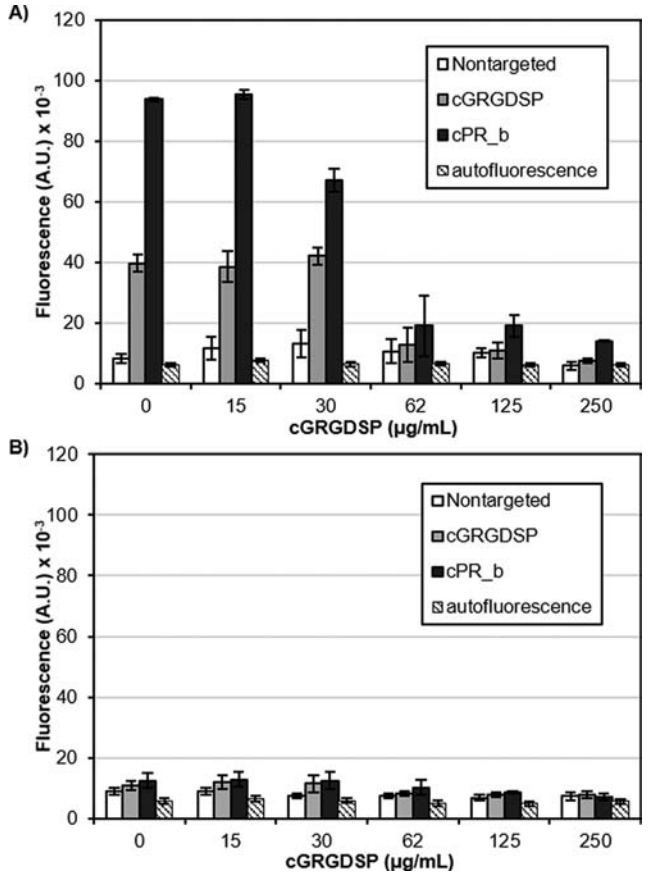

Figure 4. Specificity of targeting to the $\alpha_5\beta_1$ integrin was evaluated using polymersomes encapsulating 2 mM sulforhodamine B without a targeting group, with 9 mol % cGRGDSP, or with 9 mol % cPR_b incubated with either (A) high $\alpha_5\beta_1$-expressing DLD-1 cells or (B) low $\alpha_5\beta_1$-expressing CACO-2 cells. Increasing concentrations of free cGRGDSP peptide were added prior to incubation to determine if binding between integrins and fluorescent polymersomes could be blocked. Following 1 h incubation at 37 °C, unbound polymersomes were washed away and the fluorescence of bound polymersomes was measured. Autofluorescence of cells was measured using untreated cells. Data are the mean ± standard error of 3 separate experiments ($n = 3$), with each experiment performed in quadruplicate.

delivery vehicle as it is trafficked from outside the cell to different organelles following endocytosis.[88−91] Fluorescent sulforhodamine B was loaded into polymersomes at self-quenching (100 mM) concentrations, unencapsulated dye was removed, and fluorescence was tracked for 24 h by monitoring increasing fluorescence as dye escaped polymersomes. The remainder of the dye was then released to determine the fluorescence corresponding to 100% escape. After 24 h, release was nearly complete in all cases with little influence of pH on release kinetics. The release profile was well-described by first-order release kinetics over the entirety of the experiment. Consistent with previous reports, no polymer degradation was observed spectroscopically or chromatographically (Supporting Information, Figure S1), suggesting that the release mechanism in this pH range is not polymer degradation and that dye release is likely due to diffusion of the dye through the polymersome membrane.[92,93]

While simple buffered solutions can simulate the pH encountered following uptake, the absence of digestive enzymes limits the conclusions that can be drawn.[94−96] To address this limitation, release was monitored for 24 h from PEO-PMCL polymersomes following binding to DLD-1 human colon cancer cells (Figure 5B). As in binding studies (Figure 4), the total amount of delivered dye was enhanced with targeted polymersomes and cPR_b peptide outperformed cGRGDSP. After 24 h most of the dye had been released, consistent with the solution release study (Figure 5A). However, in the absence of chloroquine, release in cells is much more rapid, with >75% of the dye released within 2 h.

Dye release was also tracked in the presence of 500 μM chloroquine, a concentration verified to be nontoxic to DLD-1 cells (Supporting Information, Figure S4). This small-molecule drug is membrane-permeable at neutral pH, yet upon entering an acidic cellular compartment is protonated, rendering it membrane-impermeable and resulting in rapid accumulation of drug. This protonation raises compartment pH, decreasing the activity of hydrolases in acidic organelles such as the late endosome and lysosome.[97−100]

As shown in Figure 5B, if enzymes are not inhibited, release rates in the presence of cells are substantially faster than release rates observed in solution (Figure 5A). For example, in the case of cPR_b-targeted polymersomes, after 2 h approximately 80% release has occurred in the presence of uninhibited (0 μm chloroquine) DLD-1 cells while approximately 30% release has occurred in simple buffered solution. However, when digestive enzymes are inhibited (500 μm chloroquine) during delivery of the same polymersome formulation to DLD-1 cells approximately 35% of dye has been released after 2 h, nearly recovering solution release rates. Similar trends in relative

dx.doi.org/10.1021/bc3003259 | Bioconjugate Chem. 2013, 24, 533−543

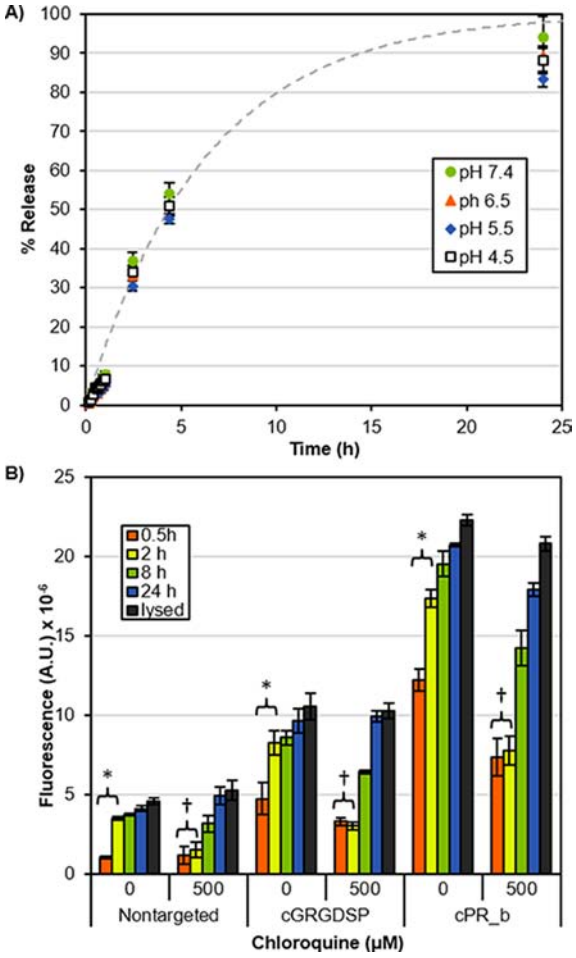

Figure 5. To measure release, polymersomes were loaded with self-quenching (100 mM) concentrations of sulforhodamine B. Release was first evaluated (A) in isotonic phosphate-citrate buffer at 37 °C with pH 7.4, typical of circulating blood, to 4.5, typical of lysosomes. No significant difference was observed in release rate at different pHs. (B) To determine if release rates changed following cell binding and uptake, polymersomes containing 100 mM sulforhodamine B were incubated for 1 h at 37 °C with DLD-1 cells with or without chloroquine. Cells were washed with 37 °C PBS and sulforhodamine B release was monitored for up to 24 h. Release in the first 2 h was much faster than observed in solution release experiments in (A) but could be inhibited by chloroquine. After 24 h nearly complete release of dye had occurred with or without chloroquine, consistent with results observed in simple buffered solutions (A). Total dye delivery was enhanced by the presence of targeting peptides, particularly cPR_b, and chloroquine had no significant effect on total dye delivered, as total fluorescence following lysis were not significantly different between untreated samples and those treated with chloroquine. In both figures, data is the mean ± standard error of 3 separate experiments (n = 3), with each experiment performed in quadruplicate. * = statistically significant difference (p < 0.02), † = no statistical significant difference (p > 0.10) *via* paired t test.

release rates between inhibited and uninhibited cells can also be observed for nontargeted and cGRGDSP-targeted polymersomes.

The rapid dye release seen in uninhibited cells was dramatically slowed upon inhibition, suggesting that acidic conditions are necessary but not sufficient for rapid release and that enzymatic hydrolases play a major role in compromising polymersomes to rapidly release the encapsulated dye. By hydrolyzing the labile ester linkages in the PMCL block, curvature is induced in the polymersome membrane resulting in pore formation and payload release, a phenomenon observed to be active in triggering payload release in other degradable polymersomal delivery systems subject to hydrolysis.[15,16,101]

To better understand the trafficking and release of dye from polymersomes, live-cell confocal microscopy was used to directly visualize trafficking and release in DLD-1 cells transfected to express both Rab5-GFP and LAMP1-RFP, markers of early endosomes and lysosomes, respectively. Labeling of organelles using these fusion proteins allowed more selective labeling of organelles than is possible using more conventional dyes that rely upon accumulation in acidic organelles. Polymersomes encapsulating 5 mM calcein blue were administered in growth media for 2 h, unbound polymersomes washed away with warm growth media, and cells imaged either immediately or 22 h later. The rapid image collection allowed by spinning disc confocal microscopy allowed visualization of trafficking in live cells in real time (Movies S1 and S2, Supporting Information), but for analysis of colocalization still frames were used.

To study trafficking, calcein blue was encapsulated at a nonquenching concentration (5 mM, Figure 6), allowing visualization of concentrated dye regardless of release. The Manders coefficients were calculated after 2 and 24 h (Table 2), allowing a quantitative evaluation of colocalization.[83,84] Here M_1 describes the portion of blue from dye delivered in polymersomes that overlaps with endosomes (green) or lysosomes (red) while M_2 describes the portion of the green or red channels that overlaps with blue. The values shown in Table 2 indicate that at early time points polymersomes have been trafficked to both the endosomes and the lysosomes. However, after 24 h the dye is predominantly colocalized with lysosomes. This result is consistent with previous reports of intracellular trafficking following binding to the $\alpha_5\beta_1$ integrin.[63,90,91]

By encapsulating a self-quenching concentration of calcein blue into polymersomes (100 mM), it was possible to track where the payload was released, as the dye will only be visible when diluted by release from the polymersomes. As in trafficking studies, colocalization was quantitatively determined using the Manders coefficients at 2 and 24 h (Table 2). In contrast to the nonquenching experiment shown in Figure 6 where some colocalization was observed between the early endosomes and the dye at early time points, for the quenching concentrations most colocalization of the dye was observed in the lysosomes even at 2 h. This trend is especially pronounced after 24 h, with very little colocalization between the early endosomes and calcein blue and more pronounced accumulations of blue dye within lysosomes. This release in the lysosomes (and to a lesser extent in the early endosomes) after 2 h is in keeping with the release rates shown in Figure 5 and further emphasizes the key role that digestive enzymes play in release of encapsulated payloads from delivery vehicles.

The observed rapid release is in stark contrast to the much slower release rate observed even at low pH in simple buffered solution, underscoring the role of enzymatic activity on intracellular payload release. Further, the fact that in Table 2 not all blue fluorescence from polymersomes overlaps with endosomes or lysosomes, particularly at later time points, suggests that the entire payload is not ultimately sequestered in these organelles. Nonetheless, given the low expected fluorescence of dye dispersed in the cytosol, definitively establishing escape from the endosomal–lysosomal degradation

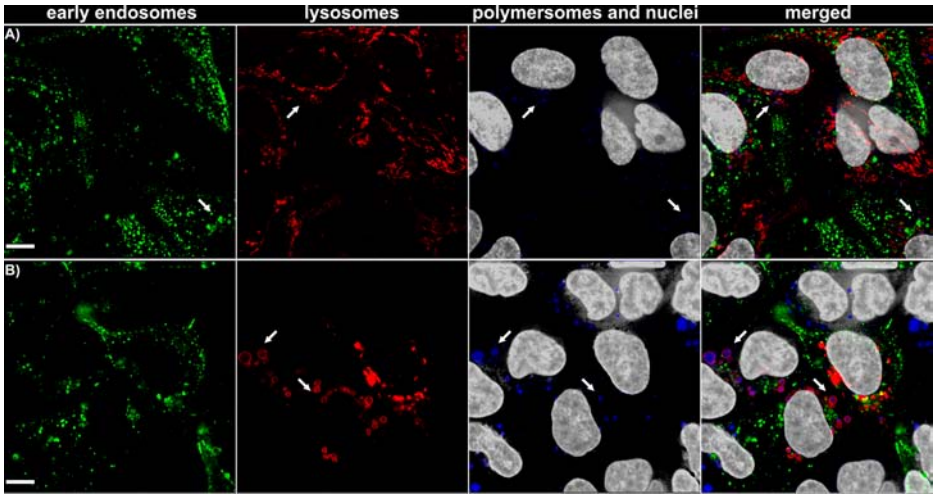

Figure 6. Confocal microscopy was used to visualize polymersome trafficking in live DLD-1 cells. Early endosomes were labeled green, lysosomes red, and nuclei stained using Hoechst 33342 (nuclei color removed to aid interpretation). Polymersomes were blue due to encapsulated calcein blue dye at a nonquenching concentration (5 mM), allowing tracking of the carriers. The polymersomes were incubated with the cells for 2 h at 37 °C. The cells were washed and images were collected immediately (A) or 22 h later (B). Scale bars indicate 10 μm and arrows are included to aid in identifying some areas of colocalization.

Table 2. Manders Coefficients Were Determined for cPR_b-Functionalized Polymersomes Delivered to DLD-1 Cells (shown in Figures 6 and 7) to Quantitatively Describe Colocalization between the Blue Channel (Polymersomes) and Either the Green (Early Endosomes) or Red (Lysosomes) Channels after 2 and 24 h.[83,84a]

time	channel	M_1	M_2	dye
2 h	green	0.3792	0.0402	5 mM
2 h	red	0.6405	0.0719	5 mM
24 h	green	0.0455	0.0211	5 mM
24 h	red	0.8452	0.1948	5 mM
2 h	green	0.0824	0.0337	100 mM
2 h	red	0.8694	0.4686	100 mM
24 h	green	0.0186	0.0902	100 mM
24 h	red	0.9290	0.1886	100 mM

[a] M_1 describes the portion of the blue channel that overlaps with either the red or the green channel while M_2 describes the portion of the red or green channel that overlaps with the blue channel. Nonquenching dye concentrations (5 mM) were used to study trafficking while quenching concentrations (100 mM) were used to determine the location of intracellular dye release. In all calculations nuclei were omitted.

pathway on the basis of this analysis alone is challenging. This question was instead addressed by determining if a drug delivered in the polymersomes that requires delivery to the cytosol or nucleus inhibits cell growth, as only drug that is released from organelles will inhibit growth and drug sequestered in the endosomes or lysosomes would not be expected to affect viability.

Cisplatin was encapsulated into polymersomes and delivered to DLD-1 cells to determine if the enhanced binding of targeted polymersomes observed in Figure 4 and Figure 5 would yield commensurate gains in treatment efficacy. Cisplatin interacts with nucleic acids of rapidly dividing cancer cells to hinder their growth and is not expected to inhibit growth if wholly sequestered in lysosomes.[102,103] The well-established MTT viability assay was used to determine the 50% inhibition concentration (IC_{50}) of DLD-1 and CACO-2 cultures following treatment with free cisplatin or the drug encapsulated in non-, cGRGDSP-, or cPR_b-targeted polymersomes (Figure 8). Prior to cell studies polymersomes were verified to encapsulate cisplatin, with encapsulation efficiencies (3−5%) on the lower side of previous reports using polymersomes to encapsulate drugs not amenable to so-called "active" loading.[10,81,82] Following encapsulation, polymersomes were verified to release the drug quite slowly in simple buffered media (Supporting Information, Figure S6).

Free drug required the lowest dose to inhibit growth using both $\alpha_5\beta_1$-overexpressing DLD-1 cells and low $\alpha_5\beta_1$-expressing CACO-2 cells, which is attributed to the drug being able to interact with the cell without first releasing from a polymersome. In contrast, when encapsulated in nontargeted polymersomes significantly more drug was necessary to inhibit growth. Given the results of polymer toxicity studies (Figure 2), this low toxicity from the cisplatin encapsulated in the nontargeted formulations is probably the result of drug release following limited delivery *via* the same nonspecific uptake pathway that was responsible for delivery in Figure 4A and Figure 5B). When a targeting peptide was used, the enhancements to binding and payload delivery compared to the nontargeted formulations, as observed in Figure 4A and Figure 5B, resulted in decreased viability for $\alpha_5\beta_1$-overexpressing DLD-1 cells, while IC_{50} values were not significantly affected for CACO-2 cells. For DLD-1 cells, the cGRGDSP peptide was effective relative to nontargeted polymersomes while cPR_b reduced the amount of cisplatin required by more than 50% relative to the nontargeted formulation. Statistical comparison indicated no significant difference between the amounts of drug needed using cPR_b-functionalized polymersomes and free drug in DLD-1 cells. Taken together with the binding experiments shown in Figure 4 it can be seen that targeting with the cPR_b peptide not only enhanced binding to $\alpha_5\beta_1$-overexpressing cells and delivery of the encapsulated drug but it also left almost unaffected cells with low levels of the targeted $\alpha_5\beta_1$ integrin receptor.

A substantial difference is apparent between relative binding, as seen in Figure 4, and relative growth inhibition, as observed in the IC_{50} results shown in Figure 8. This difference is consistent with microscopy (Figure 5 and Figure 6) which

dx.doi.org/10.1021/bc3003259 | *Bioconjugate Chem.* 2013, 24, 533−543

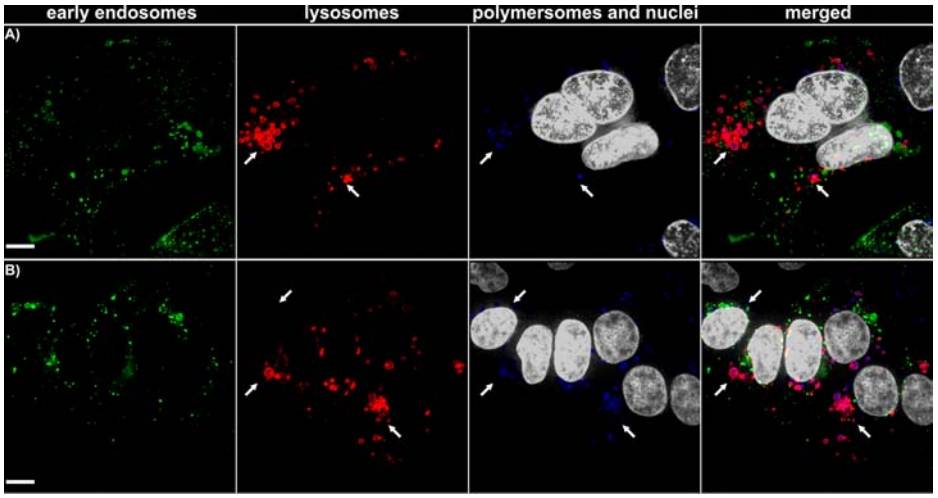

Figure 7. Confocal microscopy was used to visualize polymersome release in live DLD-1 cells. Early endosomes were labeled green, lysosomes were labeled red, and nuclei were lightly stained using Hoechst 33342 (nucleus color was removed to aid interpretation). Polymersomes were blue due to encapsulating calcein blue at quenching concentrations (100 mM), allowing tracking of released dye. Cells were incubated with polymersomes for 2 h at 37 °C, unbound polymersomes washed away with warm GM, and images collected immediately (A) or after 22 h (B). Scale bars indicate 10 μm and arrows are included to aid in identifying colocalization but are not the only regions of colocalization.

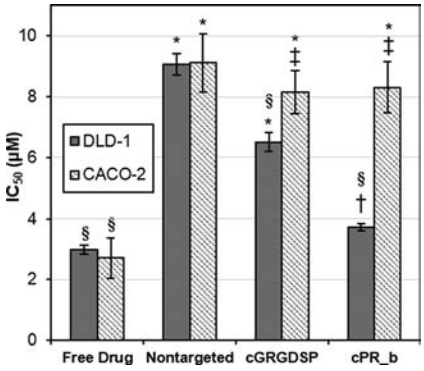

Figure 8. The IC_{50} value for free cisplatin, nontargeted polymersomes, cGRGDSP-functionalized polymersomes (9 mol % cGRGDSP), and cPR_b-functionalized polymersomes (9 mol % cPR_b) was determined for DLD-1 cells following incubation for 24 h at 37 °C. Free cisplatin had the lowest IC_{50}, followed closely by cisplatin encapsulated in targeted polymersomes using the cPR_b peptide. Significantly more drug was necessary to inhibit cell growth when encapsulated in cGRGDSP-functionalized polymersomes, while approximately three times more cisplatin was required to inhibit cell growth when encapsulated in nontargeted polymersomes compared to free drug. In contrast, delivery to the CACO-2 cell line showed no significant difference from the nontargeted polymersomes regardless of the targeting peptide. Results (mean ± standard error) for the DLD-1 are from four separate experiments ($n = 4$) each conducted in triplicate and results for the CACO-2 are from three separate experiments ($n = 3$) each conducted in triplicate. * statistically significant difference from free drug ($p < 0.05$), † no statistical difference from free drug ($p > 0.10$), § statistically significant difference from nontargeted polymersomes ($p < 0.05$), ‡ no statistical difference from nontargeted polymersomes ($p > 0.10$) *via* paired *t* test.

indicated that a substantial fraction of the polymersomes' payload was delivered to the lysosomes, where it is physically sequestered away from nuclear DNA to which it would otherwise bind to inhibit cellular function and growth.[25,104−107] Nonetheless, the effectiveness of cisplatin delivery using targeted polymersomes suggests that the lysosome is not the only site of their delivery and release, as sufficient quantities of the cisplatin drug must be escaping from polymersomes and lysosomes following their uptake in order to see the observed growth inhibition.

CONCLUSIONS

Cisplatin therapy is often limited by major side effects and resistance. By tethering the cPR_b targeting peptide to the outside of PEO-PMCL polymersomes it was possible to obtain specific binding and uptake into $\alpha_5\beta_1$-overexpressing human colon cancer cells, greatly exceeding the amount of binding seen with a cGRGDSP ligand while maintaining minimal binding to cells with low levels of $\alpha_5\beta_1$ expression. Intracellular release was tracked and imaged by a combination of fluorescent plate assays and live-cell confocal microscopy. The effect of pH alone on polymer degradation and payload release rates was found to be minimal from pH 7.4 to 4.5. Release occurred much more rapidly following endocytosis and the slower solution release rates could be recovered by inhibiting enzymes in acidic organelles, implicating enzymatic hydrolysis as a key mode of release for PEO-PMCL polymersomes. When cPR_b-functionalized polymersomes were used to encapsulate cisplatin, toxicity to $\alpha_5\beta_1$-overexpressing cells outperformed nontargeted and cGRGDSP-functionalized polymersomes, with IC_{50} values on par with those of the free drug, while maintaining low levels of toxicity to cells expressing low levels of the integrin. PEO-PMCL polymersomes with PR_b targeting appear to be promising carriers for minimizing side effects due to nonspecific delivery into $\alpha_5\beta_1$-overexpressing cancer cells.

ASSOCIATED CONTENT

Supporting Information

Degradation data on PEO-PMCL polymersomes in buffered solution, CAC measurement, NTA size characterization, chloroquine toxicity, representative IC_{50} measurements, release rates for cisplatin from polymersomes, and movie of polymersomes in early endosomes and lysosomes in live cells. This material is available free of charge via the Internet at http://pubs.acs.org.

dx.doi.org/10.1021/bc3003259 | *Bioconjugate Chem.* 2013, 24, 533−543

AUTHOR INFORMATION

Corresponding Author

*E-mail: kokkoli@umn.edu (E.K.).

Notes

The authors declare no competing financial interest.

ACKNOWLEDGMENTS

This work was supported primarily by the MRSEC Program of the National Science Foundation under award number DMR-0819885.

REFERENCES

(1) Pangburn, T. O., Petersen, M. A., Waybrant, B., Adil, M. M., and Kokkoli, E. (2009) Peptide- and aptamer-functionalized nanovectors for targeted delivery of therapeutics. *Journal of Biomechanical Engineering 131*, 74005.

(2) Cho, K., Wang, X., Nie, S., Chen, Z., and Shin, D. M. (2008) Therapeutic nanoparticles for drug delivery in cancer. *Clin. Cancer Res. 14*, 1310−1316.

(3) Liu, Y., Miyoshi, H., and Nakamura, M. (2007) Nanomedicine for drug delivery and imaging: a promising avenue for cancer therapy and diagnosis using targeted functional nanoparticles. *Int. J. Cancer 120*, 2527−2537.

(4) Pearce, T. R., Shroff, K., and Kokkoli, E. (2012) Peptide targeted lipid nanoparticles for anticancer drug delivery. *Adv. Mater. 24*, 3803−3822.

(5) Unezaki, S., Maruyama, K., Hosoda, J.-I., Nagae, I., Koyanagi, Y., Nakata, M., Ishida, O., Iwatsuru, M., and Tsuchiya, S. (1996) Direct measurement of the extravasation of polyethyleneglycol-coated liposomes into solid tumor tissue by in vivo fluorescence microscopy. *Int. J. Pharm. 144*, 11−17.

(6) Lasic, D. D., and Needham, D. (1995) The "stealth" liposome: a prototypical biomaterial. *Chem. Rev. 95*, 2601−2628.

(7) Maeda, H., Wu, J., Sawa, T., Matsumura, Y., and Hori, K. (2000) Tumor vascular permeability and the EPR effect in macromolecular therapeutics: a review. *J. Controlled Release 65*, 271−284.

(8) Discher, B. M., Won, Y. Y., Ege, D. S., Lee, J. C.-M., Bates, F. S., Discher, D. E., and Hammer, D. A. (1999) Polymersomes: tough vesicles made from diblock copolymers. *Science 284*, 1143−1146.

(9) Photos, P. J., Bacakova, L., Discher, B., Bates, F. S., and Discher, D. E. (2003) Polymer vesicles in vivo: correlations with PEG molecular weight. *J. Controlled Release 90*, 323−334.

(10) Lee, J. C.-M., Bermudez, H., Discher, B. M., Sheehan, M. A., Won, Y.-Y., Bates, F. S., and Discher, D. E. (2001) Preparation, stability, and in vitro performance of vesicles made with diblock copolymers. *Biotechnol. Bioeng. 73*, 135−145.

(11) Discher, D. E., and Ahmed, F. (2006) Polymersomes. *Annu. Rev. Biomed. Eng. 8*, 323−341.

(12) Demirgöz, D., Pangburn, T. O., Davis, K. P., Lee, S., Bates, F. S., and Kokkoli, E. (2009) PR_b-targeted delivery of tumor necrosis factor-α by polymersomes for the treatment of prostate cancer. *Soft Matter 5*, 2011−2019.

(13) Ahmed, F., Pakunlu, R. I., Srinivas, G., Brannan, A., Bates, F., Klein, M. L., Minko, T., and Discher, D. E. (2006) Shrinkage of a rapidly growing tumor by drug-loaded polymersomes: pH-triggered release through copolymer degradation. *Mol. Pharmaceutics 3*, 340−350.

(14) Geng, Y., and Discher, D. E. (2005) Hydrolytic degradation of poly(ethylene oxide)-block-polycaprolactone worm micelles. *J. Am. Chem. Soc. 127*, 12780−12781.

(15) Ahmed, F., and Discher, D. E. (2004) Self-porating polymersomes of PEG-PLA and PEG-PCL: hydrolysis-triggered controlled release vesicles. *J. Controlled Release 96*, 37−53.

(16) Ghoroghchian, P. P., Li, G., Levine, D. H., Davis, K. P., Bates, F. S., Hammer, D. A., and Therien, M. J. (2006) Bioresorbable vesicles formed through spontaneous self-assembly of amphiphilic poly(ethylene oxide)-block-polycaprolactone. *Macromolecules 39*, 1673−1675.

(17) Vangeyte, P., Leyh, B., Heinrich, M., Grandjean, J., Bourgaux, C., and Jerome, R. (2004) Self-assembly of poly(ethylene oxide)-b-poly(ε-caprolactone) copolymers in aqueous solution. *Langmuir 20*, 8442−8451.

(18) Meng, F., Hiemstra, C., Engbers, G. H. M., and Feijen, J. (2003) Biodegradable polymersomes. *Macromolecules 36*, 3004−3006.

(19) Upadhyay, K. K., Bhatt, A. N., Mishra, A. K., Dwarakanath, B. S., Jain, S., Schatz, C., Le Meins, J.-F., Farooque, A., Chandraiah, G., Jain, A. K., Misra, A., and Lecommandoux, S. (2010) The intracellular drug delivery and anti-tumor activity of doxorubicin loaded poly(γ-benzyl L-glutamate)-b-hyaluronan polymersomes. *Biomaterials 31*, 2882−2892.

(20) Petersen, M. A., Yin, L., Kokkoli, E., and Hillmyer, M. A. (2010) Synthesis and characterization of reactive PEO−PMCL polymersomes. *Polym. Chem. 1*, 1281−1290.

(21) Zupancich, J. A., Bates, F. S., and Hillmyer, M. A. (2006) Aqueous dispersions of poly(ethylene oxide)-b-poly(γ-methyl-ε-caprolactone) block copolymers. *Macromolecules 39*, 4286−4288.

(22) Zupancich, J. A., Bates, F. S., and Hillmyer, M. A. (2009) Synthesis and self-assembly of RGD-functionalized PEO-PB amphiphiles. *Biomacromolecules 10*, 1554−1563.

(23) Barabas, K., Milner, R., Lurie, D., and Adin, C. (2008) Cisplatin: a review of toxicities and therapeutic applications. *Vet. Comp. Oncol. 6*, 1−18.

(24) Stewart, D. J., Benjamin, R. S., Luna, M., Feun, L., Caprioli, R., Seifert, W., and Loo, T. L. (1982) Human tissue distribution of platinum after cis-diamminedichloroplatinum. *Cancer Chemother. Pharmacol. 10*, 51−54.

(25) Siddik, Z. H. (2003) Cisplatin: mode of cytotoxic action and molecular basis of resistance. *Oncogene 22*, 7265−7279.

(26) Perez, R. P. (1998) Cellular and molecular determinants of cisplatin resistance. *Eur. J. Cancer 34*, 1535−1542.

(27) Haxton, K. J., and Burt, H. M. (2009) Polymeric drug delivery of platinum-based anticancer agents. *J. Pharm. Sci. 98*, 2299−2316.

(28) Sanchez-Cano, C., and Hannon, M. J. (2009) Novel and emerging approaches for the delivery of metallo-drugs. *Dalton Trans. 48*, 10702−10711.

(29) Peleg-Shulman, T., Gibson, D., Cohen, R., Abra, R., and Barenholz, Y. (2001) Characterization of sterically stabilized cisplatin liposomes by nuclear magnetic resonance. *Biochim. Biophys. Acta 1510*, 278−291.

(30) Working, P. K., Newman, M. S., Sullivan, T., Brunner, M., Podell, M., Sahenk, Z., and Turner, N. (1998) Comparative intravenous toxicity of cisplatin solution and cisplatin encapsulated in long-circulating, pegylated liposomes in cynomolgus monkeys. *Toxicol. Sci. 46*, 155−165.

(31) Zamboni, W. C., Gervais, A. C., Egorin, M. J., Schellens, J. H. M., Zuhowski, E. G., Pluim, D., Joseph, E., Hamburger, D. R., Working, P. K., and Colbern, G. (2004) Systemic and tumor disposition of platinum after administration of cisplatin or STEALTH liposomal-cisplatin formulations (SPI-077 and SPI-077 B103) in a preclinical tumor model of melanoma. *Cancer Chemother. Pharmacol. 53*, 329−336.

(32) Newman, M. S., Colbern, G. T., Working, P. K., Engbers, C., and Amantea, M. A. (1999) Comparative pharmacokinetics, tissue distribution, and therapeutic effectiveness of cisplatin encapsulated in long-circulating, pegylated liposomes (SPI-077) in tumor-bearing mice. *Cancer Chemother. Pharmacol. 43*, 1−7.

(33) Bandak, S., Goren, D., Horowitz, A., Tzemach, D., and Gabizon, A. (1999) Pharmacological studies of cisplatin encapsulated in long-circulating liposomes in mouse tumor models. *Anti-Cancer Drugs 10*, 911−920.

(34) Rosenthal, D. I., Yom, S. S., Liu, L., Machtay, M., Algazy, K., Weber, R. S., Weinstein, G. S., Chalian, A. A., Miller, L. K., Rockwell, K., Tonda, M., Schnipper, E., and Hershock, D. (2002) A Phase I study of SPI-077 (Stealth® liposomal cisplatin) concurrent with radiation therapy for locally advanced head and neck cancer. *Invest. New Drugs 20*, 343−349.

(35) White, S. C., Lorigan, P., Margison, G. P., Margison, J., M. Martin, F., Thatcher, N., Anderson, H., and Ranson, M. (2006) Phase II study of SPI-77 (sterically stabilised liposomal cisplatin) in advanced non-small-cell lung cancer. *Br. J. Cancer 95*, 822−828.
(36) Harrington, K. J., Lewanski, C. R., Northcote, A. D., Whittaker, J., Wellbank, H., Vile, R. G., Peters, A. M., and Stewart, J. S. W. (2001) Phase I-II study of pegylated liposomal cisplatin (SPI-077 TM) in patients with inoperable head and neck cancer. *Ann. Oncol. 12*, 493−496.
(37) Seetharamu, N., Kim, E., Hochster, H., Martin, F., and Muggia, F. (2010) Phase II study of liposomal cisplatin (SPI-77) in platinum-sensitive recurrences of ovarian cancer. *Anticancer Res. 30*, 541−546.
(38) Ohmichi, M., Hayakawa, J., Tasaka, K., Kurachi, H., and Murata, Y. (2005) Mechanisms of platinum drug resistance. *Trends Pharmacol. Sci. 26*, 113−116.
(39) Iinuma, H., Maruyama, K., Okinaga, K., Sasaki, K., Sekine, T., Ishida, O., Ogiwara, N., Johkura, K., and Yonemura, Y. (2002) Intracellular targeting therapy of cisplatin-encapsulated transferrin-polyethylene glycol liposome on peritoneal dissemination of gastric cancer. *Int. J. Cancer 99*, 130−137.
(40) Krieger, M. L., Eckstein, N., Schneider, V., Koch, M., Royer, H.-D., Jaehde, U., and Bendas, G. (2010) Overcoming cisplatin resistance of ovarian cancer cells by targeted liposomes in vitro. *Int. J. Pharm. 389*, 10−17.
(41) Mai, J., Song, S., Rui, M., Liu, D., Ding, Q., Peng, J., and Xu, Y. (2009) A synthetic peptide mediated active targeting of cisplatin liposomes to Tie2 expressing cells. *J. Controlled Release 139*, 174−181.
(42) Dhar, S., Gu, F. X., Langer, R., Farokhzad, O. C., and Lippard, S. J. (2008) Targeted delivery of cisplatin to prostate cancer cells by aptamer functionalized Pt(IV) prodrug-PLGA−PEG nanoparticles. *Proc. Natl. Acad. Sci. U.S.A. 105*, 17356−17361.
(43) Cao, Z., Tong, R., Mishra, A., Xu, W., Wong, G. C. L., Cheng, J., and Lu, Y. (2009) Reversible cell-specific drug delivery with aptamer-functionalized liposomes. *Angew. Chem., Int. Ed. 48*, 6494−6498.
(44) Mukhopadhyay, S., Barnés, C. M., Haskel, A., Short, S. M., Barnes, K. R., and Lippard, S. J. (2007) Conjugated platinum(IV)−peptide complexes for targeting angiogenic tumor vasculature. *Bioconjugate Chem. 19*, 39−49.
(45) Levine, R. M., Scott, C. M., and Kokkoli, E. (2013) Peptide functionalized nanoparticles for nonviral gene delivery. *Soft Matter 9*, 985−1004.
(46) Pierschbacher, M. D., and Ruoslahti, E. (1984) Cell attachment activity of fibronectin can be duplicated by small synthetic fragments of the molecule. *Nature 309*, 30−33.
(47) Ruoslahti, E., and Pierschbacher, M. D. (1987) New perspectives in cell adhesion: RGD and integrins. *Science 238*, 491−497.
(48) Kokkoli, E., Mardilovich, A., Wedekind, A., Rexeisen, E. L., Garg, A., and Craig, J. A. (2006) Self-assembly and applications of biomimetic and bioactive peptide-amphiphiles. *Soft Matter 2*, 1015−1024.
(49) Muschler, J. L., and Horwitz, A. F. (1991) Down-regulation of the chicken $\alpha_5\beta_1$ integrin fibronectin receptor during development. *Development 113*, 327−37.
(50) Van Golen, K. L., Bao, L., Brewer, G. J., Pienta, K. J., Kamradt, J. M., Livant, D. L., and Merajver, S. D. (2002) Suppression of tumor recurrence and metastasis by a combination of the PHSCN sequence and the antiangiogenic compound tetrathiomolybdate in prostate carcinoma. *Neoplasia 4*, 373−379.
(51) Gong, J., Wang, D. H., Sun, L. Z., Zborowska, E., Wilson, J. K. V., and Brattain, M. G. (1997) Role of $\alpha_5\beta_1$ integrin in determining malignant properties of colon carcinoma cells. *Cell Growth Different. 8*, 83−90.
(52) Jayne, D. G., Heath, R. M., Dewhurst, O., Scott, N., and Guillou, P. J. (2002) Extracellular matrix proteins and chemoradiotherapy: $\alpha_5\beta_1$ integrin as a predictive marker in rectal cancer. *Eur. J. Surg. Oncol. 28*, 30−36.
(53) Ellis, L. M. (2003) A Targeted approach for antiangiogenic therapy of metastatic human colon cancer. *Am. Surg. 69*, 3−10.
(54) Jia, Y., Zeng, Z.-Z., Markwart, S. M., Rockwood, K. F., Ignatoski, K. M. W., Ethier, S. P., and Livant, D. L. (2004) Integrin fibronectin receptors in matrix metalloproteinase-1-dependent invasion by breast cancer and mammary epithelial cells. *Cancer Res. 64*, 8674−8681.
(55) Chen, J., De, S., Brainard, J., and Byzova, T. V. (2004) Metastatic properties of prostate cancer cells are controlled by VEGF. *Cell Commun. Adhes. 11*, 1−11.
(56) Maglott, A., Bartik, P., Cosgun, S., Klotz, P., Rondé, P., Fuhrmann, G., Takeda, K., Martin, S., and Dontenwill, M. (2006) The small $\alpha_5\beta_1$ integrin antagonist, SJ749, reduces proliferation and clonogenicity of human astrocytoma cells. *Cancer Res. 66*, 6002−6007.
(57) Mizejewski, G. J. (1999) Role of integrins in cancer: survey of expression patterns. *Proc. Soc. Exp. Biol. Med. 222*, 124−138.
(58) Dingemans, A.-M. C., Van den Boogaart, V., Vosse, B. A., Van Suylen, R.-J., Griffioen, A. W., and Thijssen, V. L. (2010) Integrin expression profiling identifies integrin α_5 and β_1 as prognostic factors in early stage non-small cell lung cancer. *Mol. Cancer 9*, 152.
(59) Craig, J. A., Rexeisen, E. L., Mardilovich, A., Shroff, K., and Kokkoli, E. (2008) Effect of linker and spacer on the design of a fibronectin-mimetic peptide evaluated via cell studies and AFM adhesion forces. *Langmuir 24*, 10282−10292.
(60) Mardilovich, A., and Kokkoli, E. (2004) Biomimetic peptide-amphiphiles for functional biomaterials: the role of GRGDSP and PHSRN. *Biomacromolecules 5*, 950−957.
(61) Mardilovich, A., and Kokkoli, E. (2005) Patterned biomimetic membranes: effect of concentration and pH. *Langmuir 21*, 7468−7475.
(62) Mardilovich, A., Craig, J. A., McCammon, M. Q., Garg, A., and Kokkoli, E. (2006) Design of a novel fibronectin-mimetic peptide-amphiphile for functionalized biomaterials. *Langmuir 22*, 3259−3264.
(63) Pangburn, T. O., Bates, F. S., and Kokkoli, E. (2012) Polymersomes functionalized via "click" chemistry with the fibronectin mimetic peptides PR_b and GRGDSP for targeted delivery to cells with different levels of $\alpha_5\beta_1$ expression. *Soft Matter 8*, 4449−4461.
(64) Shroff, K., Pearce, T. R., and Kokkoli, E. (2011) Enhanced integrin mediated signaling and cell cycle progression on fibronectin mimetic peptide amphiphile monolayers. *Langmuir 28*, 1858−1865.
(65) Demirgöz, D., Garg, A., and Kokkoli, E. (2008) PR_b-Targeted PEGylated liposomes for prostate cancer therapy. *Langmuir 24*, 13518−13524.
(66) Garg, A., Tisdale, A. W., Haidari, E., and Kokkoli, E. (2009) Targeting colon cancer cells using PEGylated liposomes modified with a fibronectin-mimetic peptide. *Int. J. Pharm. 366*, 201−210.
(67) Garg, A., and Kokkoli, E. (2011) pH-Sensitive PEGylated liposomes functionalized with a fibronectin-mimetic peptide show enhanced intracellular delivery to colon cancer cells. *Curr. Pharm. Biotechnol. 12*, 1135−1143.
(68) Atchison, N. A., Fan, W., Papas, K. K., Hering, B. J., Tsapatsis, M., and Kokkoli, E. (2010) Binding of the fibronectin-mimetic peptide, PR_b, to $\alpha_5\beta_1$ on pig islet cells increases fibronectin production and facilitates internalization of PR_b functionalized liposomes. *Langmuir 26*, 14081−14088.
(69) Shroff, K., and Kokkoli, E. (2012) PEGylated liposomal doxorubicin targeted to $\alpha_5\beta_1$-expressing MDA-MB-231 breast cancer cells. *Langmuir 28*, 4729−4736.
(70) Pangburn, T. O., Georgiou, K., Bates, F. S., and Kokkoli, E. (2012) Targeted polymersome delivery of siRNA induces cell death of breast cancer cells dependent upon Orai3 protein expression. *Langmuir 28*, 12816−12830.
(71) Adil, M., Belur, L., Pearce, T. R., Levine, R. M., Tisdale, A. W., Sorenson, B. R., McIvor, R. S., and Kokkoli, E. (2013) PR_b functionalized stealth liposomes for targeted delivery to metastatic colon cancer. *Biomater. Sci. 1*, 393−401.
(72) Kuwada, S. K., and Li, X. (2000) Integrin $\alpha_5\beta_1$ mediates fibronectin-dependent epithelial cell proliferation through epidermal growth factor receptor activation. *Mol. Biol. Cell 11*, 2485−2496.
(73) Honoré, S., Pichard, V., Penel, C., Rigot, V., Prévôt, C., Marvaldi, J., Briand, C., and Rognoni, J.-B. (2000) Outside-in regulation of integrin clustering processes by ECM components per

se and their involvement in actin cytoskeleton organization in a colon adenocarcinoma cell line. *Histochem. Cell Biol. 114*, 323−335.
(74) Croyle, M. A., Walter, E., Janich, S., Roessler, B. J., and Amidon, G. L. (1998) Role of integrin expression in adenovirus-mediated gene delivery to the intestinal epithelium. *Hum. Gene Ther. 9*, 561−572.
(75) Kozlova, N. I., Morozevich, G. E., Chubukina, A. N., and Berman, A. E. (2001) Integrin $\alpha v\beta_3$ promotes anchorage-dependent apoptosis in human intestinal carcinoma cells. *Oncogene 20*, 4710−4717.
(76) Hidalgo, I. J., Raub, T. J., and Borchardt, R. T. (1989) Characterization of the human colon carcinoma cell line (Caco-2) as a model system for intestinal epithelial permeability. *Gastroenterology 96*, 736−749.
(77) Press, B., and Di Grandi, D. (2008) Permeability for intestinal absorption: Caco-2 assay and related issues. *Curr. Drug Metab. 9*, 893−900.
(78) Birtwistle, M. R., and Kholodenko, B. N. (2009) Endocytosis and signalling: a meeting with mathematics. *Mol. Oncol. 3*, 308−320.
(79) Vangeyte, P., and Jérôme, R. (2004) Amphiphilic block copolymers of high-molecular-weight poly(ethylene oxide) and either ε-caprolactone or γ-methyl-ε-caprolactone: synthesis and characterization. *J. Polym. Sci., Part A: Polym. Chem. 42*, 1132−1142.
(80) Golla, E. D. (1973) Spectrophotometric determination of platinum with o-phenylenediamine. *Talanta 20*, 199−210.
(81) Onaca, O., Nallani, M., Ihle, S., Schenk, A., and Schwaneberg, U. (2006) Functionalized nanocompartments (synthosomes): limitations and prospective applications in industrial biotechnology. *Biotechnol. J. 1*, 795−805.
(82) Avgoustakis, K., Beletsi, A., Panagi, Z., Klepetsanis, P., Karydas, A. G., and Ithakissios, D. S. (2002) PLGA-mPEG nanoparticles of cisplatin: in vitro nanoparticle degradation, in vitro drug release and in vivo drug residence in blood properties. *J. Controlled Release 79*, 123−135.
(83) Manders, E. M. M., Verbeek, F. J., and Aten, J. A. (1993) Measurement of co-localization of objects in dual-colour confocal images. *J. Microsc. 169*, 375−382.
(84) Costes, S. V., Daelemans, D., Cho, E. H., Dobbin, Z., Pavlakis, G., and Lockett, S. (2004) Automatic and quantitative measurement of protein-protein colocalization in live cells. *Biophys. J. 86*, 3993−4003.
(85) Kirpotin, D. B., Drummond, D. C., Shao, Y., Shalaby, M. R., Hong, K., Nielsen, U. B., Marks, J. D., Benz, C. C., and Park, J. W. (2006) Antibody targeting of long-circulating lipidic nanoparticles does not increase tumor localization but does increase internalization in animal models. *Cancer Res. 66*, 6732−6740.
(86) Nair, L. S., and Laurencin, C. T. (2007) Biodegradable polymers as biomaterials. *Prog. Polym. Sci. 32*, 762−798.
(87) Sun, H., Mei, L., Song, C., Cui, X., and Wang, P. (2006) The in vivo degradation, absorption and excretion of PCL-based implant. *Biomaterials 27*, 1735−1740.
(88) Juliano, R. L., Ming, X., and Nakagawa, O. (2011) Cellular uptake and intracellular trafficking of antisense and siRNA oligonucleotides. *Bioconjugate Chem. 23*, 147−157.
(89) Mayor, S., and Pagano, R. E. (2007) Pathways of clathrin-independent endocytosis. *Nat. Rev. Mol. Cell. Biol. 8*, 603−612.
(90) Sottile, J., and Chandler, J. (2005) Fibronectin matrix turnover occurs through a caveolin-1−dependent process. *Mol. Biol. Cell 16*, 757−768.
(91) Shi, F., and Sottile, J. (2008) Caveolin-1-dependent β_1 integrin endocytosis is a critical regulator of fibronectin turnover. *J, Cell Sci. 121*, 2360−2371.
(92) Chunhua, S., Shengrong, G., and Lu., C. (2008) Degradation behaviors of monomethoxy poly(ethylene glycol)-b-poly(ε-caprolactone) nanoparticles in aqueous solution. *Polym. Adv. Technol. 19*, 66−72.
(93) Jung, J. H., Ree, M., and Kim, H. (2006) Acid- and base-catalyzed hydrolyses of aliphatic polycarbonates and polyesters. *Catal. Today 115*, 283−287.
(94) Gan, Z., Jim, T. F., Li, M., Yuer, Z., Wang, S., and Wu, C. (1999) Enzymatic biodegradation of poly(ethylene oxide-b-ε-caprolactone) diblock copolymer and its potential biomedical applications. *Macromolecules 32*, 590−594.
(95) Carstens, M. G., van Nostrum, C. F., Verrijk, R., de Leede, L. G., Crommelin, D. J., and Hennink, W. E. (2008) A mechanistic study on the chemical and enzymatic degradation of PEG-oligo(ε-caprolactone) micelles. *J. Pharm. Sci. 97*, 506−518.
(96) Lam, C. X. F., Savalani, M. M., Teoh, S.-H., and Hutmacher, D. W. (2008) Dynamics of in vitro polymer degradation of polycaprolactone-based scaffolds: accelerated versus simulated physiological conditions. *Biomed. Mater. 3*, 34108.
(97) Geisow, M. J., D'Arcy Hart, P., and Young, M. R. (1981) Temporal changes of lysosome and phagosome pH during phagolysosome formation in macrophages: studies by fluorescence spectroscopy. *J. Cell Biol. 89*, 645−652.
(98) Brown, M. S., Dana, S. E., and Goldstein, J. L. (1975) Receptor-dependent hydrolysis of cholesteryl esters contained in plasma low density lipoprotein. *Proc. Natl. Acad. Sci. U.S.A. 72*, 2925−2929.
(99) Goldstein, J. L., Brunschede, G. Y., and Brown, M. S. (1975) Inhibition of proteolytic degradation of low density lipoprotein in human fibroblasts by chloroquine, concanavalin A, and triton WR 1339. *J. Biol. Chem. 250*, 7854−7862.
(100) Wagner, E., Zatloukal, K., Cotten, M., Kirlappos, H., Mechtler, K., Curiel, D. T., and Birnstiel, M. L. (1992) Coupling of adenovirus to transferrin-polylysine/DNA complexes greatly enhances receptor-mediated gene delivery and expression of transfected genes. *Proc. Natl. Acad. Sci. U.S.A. 89*, 6099−6103.
(101) Bareford, L. M., and Swaan, P. W. (2007) Endocytic mechanisms for targeted drug delivery. *Adv. Drug Delivery Rev. 59*, 748−758.
(102) Hostetter, A. A., Osborn, M. F., and DeRose, V. J. (2012) RNA-Pt Adducts following cisplatin treatment of Saccharomyces cerevisiae. *ACS Chem. Biol. 7*, 218−225.
(103) Reedijk, J., and Lohman, P. (1985) Cisplatin: synthesis, antitumour activity and mechanism of action. *Pharm. World Sci. 7*, 173−180.
(104) Larsen, A. K., Escargueil, A. E., and Skladanowski, A. (2000) Resistance mechanisms associated with altered intracellular distribution of anticancer agents. *Pharmacol. Therapeutics 85*, 217−229.
(105) Akaboshi, M., Kawai, K., Maki, H., Akuta, K., Ujeno, Y., and Miyahara, T. (1992) The number of platinum atoms binding to DNA, RNA and protein molecules of HeLa Cells treated with cisplatin at its mean lethal concentration. *Cancer Sci. 83*, 522−526.
(106) Zhang, J., Whan, R., Hambley, T., and Begley, T. P. (2007) Platinum anticancer drugs, chemical biology of. *Wiley Encycl. Chem. Biol.*, 1−10.
(107) Klein, A. V., and Hambley, T. W. (2009) Platinum drug distribution in cancer cells and tumors. *Chem. Rev. 109*, 4911−4920.